Available online at www.sciencedirect.com

ScienceDirect

www.elsevier.com/locate/jes

JES JOURNAL OF ENVIRONMENTAL SCIENCES

www.jesc.ac.cn

Rapid degradation of dyes in water by magnetic Fe^0/Fe_3O_4/graphene composites

Shan Chong, Guangming Zhang, Huifang Tian, He Zhao*

School of Environment & Natural Resource, Renmin University of China, Beijing 100872, China. Email: chongshan@ruc.edu.cn

ARTICLE INFO

Article history:
Received 15 June 2015
Revised 3 November 2015
Accepted 4 November 2015
Available online 1 February 2016

Keywords:
Fe^0/Fe_3O_4/graphene
Magnetic
Dyes
Removal
Reduction

ABSTRACT

Magnetic Fe^0/Fe_3O_4/graphene has been successfully synthesized by a one-step reduction method and investigated in rapid degradation of dyes in this work. The material was characterized by N_2 sorption–desorption, scanning electron microscopy (SEM), Fourier transform infrared spectroscopy (FT-IR), vibrating-sample magnetometer (VSM) measurements and X-ray photoelectron spectroscopy (XPS). The results indicated that Fe^0/Fe_3O_4/graphene had a layered structure with Fe crystals highly dispersed in the interlayers of graphene, which could enhance the mass transfer process between Fe^0/Fe_3O_4/graphene and pollutants. Fe^0/Fe_3O_4/graphene exhibited ferromagnetism and could be easily separated and re-dispersed for reuse in water. Typical dyes, such as Methyl Orange, Methylene Blue and Crystal Violet, could be decolorized by Fe^0/Fe_3O_4/graphene rapidly. After 20 min, the decolorization efficiencies of methyl orange, methylene blue and crystal violet were 94.78%, 91.60% and 89.07%, respectively. The reaction mechanism of Fe^0/Fe_3O_4/graphene with dyes mainly included adsorption and enhanced reduction by the composite. Thus, Fe^0/Fe_3O_4/graphene prepared by the one-step reduction method has excellent performance in removal of dyes in water.

Introduction

Dyes are widely used in the textile, leather, paper, pharmaceutical and food industries, and dye wastewater poses a potential threat to the environment and human health due to their toxicity, lack of biodegradability and carcinogenic effects (Zhao et al., 2012a, 2014; Li et al., 2014). In particular, three major types of dyes classified according to their structures, namely phenothiazine, azo and triphenylmethane dyes, are common in dye wastewater. Therefore, removal of these dyes from wastewater has been actively studied (Chen et al., 2010; Kusic et al., 2011; Nguyen et al., 2011; Noroozi and Sorial, 2013). Due to the stability of the structures of these dyes, the current treatment technologies have limited effects on removal of dyes from water and the costs are high (Padamavathy et al., 2003; Netpradit et al., 2004). Thus, it is important to develop powerful and economical approaches to degrade phenothiazine, azo and triphenylmethane dyes in water.

Ferrous materials with graphene as carrier have attracted extensive attention due to the high activity of iron and two-dimensional structure of graphene (Wang et al., 2014a). In particular, graphene-supported zero-valent iron (Jabeen et al., 2013; Liu et al., 2014) and graphene-supported iron oxide (Guo et al., 2013; Zhang et al., 2013; Zubir et al., 2014) composites have been widely studied in removal of pollutants in water. Since graphene possesses superior electrical conductivity, favoring electron transfer (Ishigami, 2007), the graphene-supported zero-valent iron composite has shown enhanced ability for reducing heavy metals in water, such as As(V) (Wang et al., 2014b), Pb(II) (Jabeen et al., 2013), and Cr(VI) (Li et al., 2015a). Since graphene possesses high specific surface area, favoring adsorption, the graphene-supported iron oxide

* *Corresponding author*. E-mail: zgm@ruc.edu.cn (Guangming Zhang).

http://dx.doi.org/10.1016/j.jes.2015.11.022
1001-0742/

composite has enhanced ability for adsorbing organic and inorganic pollutants such as methyl orange (Li et al., 2014), fulvic acid (Li et al., 2012), and Cr(VI) (Liu et al., 2013). In order to combine the enhanced reduction and adsorption ability of the above two kinds of composites, graphene-supported compounds of zero-valent iron and iron oxide have been studied and used in removal of heavy metals in water. In particular, graphene-supported Fe^0/Fe_3O_4 showed excellent performance in removal of Cr(VI) from water, and the removal efficiency could reach 83% due to the synergistic effects of reduction and adsorption in the composite containing iron, iron oxide and graphene (Lv et al., 2014). Therefore, the Fe^0/Fe_3O_4/graphene composite is worthy of further research in water treatment.

The synthesis of Fe^0/Fe_3O_4/graphene has been carried out by the methods of stepwise reduction (Lv et al., 2014) and synchronous pyrolysis (Bhunia et al., 2012). In particular, the stepwise reduction method has been common, but the process was tedious and required a toxic chemical, hydrazine hydrate. In order to overcome the defects of these methods and maintain the good performance of Fe^0/Fe_3O_4/graphene, a one-step reduction method was proposed to simultaneously reduce Fe^{2+} and Fe_3O_4/graphene oxide to Fe^0 and Fe_3O_4/graphene, respectively. The one-step reduction method, which has been used in synthesis of Fe^0/graphene composite (Guo et al., 2012; Sun et al., 2014), has the advantages of simple operation, controllable Fe^0 loading and safety, without the need for toxic organic reagents. So far the applications of Fe^0/Fe_3O_4/graphene have all been in removal of heavy metals in water, such as Cr(VI), Pb(II), Cd(II), Hg(II) (Bhunia et al., 2012; Lv et al., 2014), and no studies have been performed in removal of organic pollutants. Based on the above analysis, the removal of organic pollutants from water using Fe^0/Fe_3O_4/graphene is worthy of study. Therefore, we used a one-step reduction method to synthesize Fe^0/Fe_3O_4/graphene, anticipating stable physical and chemical properties for the composite and excellent performance in phenothiazine, azo and triphenylmethane dye removal in water treatment.

In this work, magnetic Fe^0/Fe_3O_4/graphene has been successfully synthesized by using a one-step reduction method and investigated in removal of dyes in water. Scanning electron microscopy (SEM), Fourier transform infrared spectroscopy (FT-IR), X-ray photoelectron spectroscopy (XPS), vibrating-sample magnetometer (VSM) measurements and N_2 sorption–desorption were used to investigate the morphologic and physical/chemical properties of Fe^0/Fe_3O_4/graphene. The removal of Methyl Orange, Methylene Blue and Crystal Violet in water was assessed to evaluate the reactivity of Fe^0/Fe_3O_4/graphene. The mechanism was deduced to reveal the reaction process in Fe^0/Fe_3O_4/graphene. The aim of this study was to use a simple method to synthesize Fe^0/Fe_3O_4/graphene and use it to remove refractory dyes in water.

1. Experimental

1.1. Reagents and materials

All chemicals used in this study were of analytical grade and used without further purification. Expandable graphite was obtained from Qingdao Tianhe Graphite Co., Ltd., China. Crystal violet, Methylene Blue and Methyl Orange were obtained from Sinopharm Chemical Reagent Co., Ltd., China. Ferric chloride hexahydrate ($FeCl_3·6H_2O$), ferrous sulfate heptahydrate ($FeSO_4·7H_2O$), potassium permanganate ($KMnO_4$), sodium nitrate ($NaNO_3$), sodium borohydride ($NaBH_4$), and sodium hydroxide (NaOH) were purchased from Xilong Chemical Co., Ltd. Hydrogen peroxide (H_2O_2, 30%, V/V), ammonia solution ($NH_3·H_2O$, 28%, V/V), hydrochloric acid (HCl), and sulfuric acid (H_2SO_4, 98%) were obtained from Beijing Chemical Works, China. Nitrogen (N_2) gas was supplied by Beijing Aolin Gas Company, China. Solutions were prepared with deionized water purified by a Millipore Milli Q UV Plus system.

1.2. Synthesis of Fe^0/Fe_3O_4/graphene

1.2.1. Synthesis of graphene oxide

The preparation of graphene oxide was carried out by a hydrothermal method (Bao et al., 2012). Expandable graphite, $NaNO_3$, $KMnO_4$, H_2SO_4 (98%) and a Teflon reactor were cooled in a refrigerator at 0–4°C before use. The Teflon reactor was placed in a stainless steel autoclave. The cooled expandable graphite (1 g), $NaNO_3$ (1 g), and $KMnO_4$ (4 g) were put into the 100 ml reactor, then H_2SO_4 (50 mL) was added. As soon as the H_2SO_4 was added, the reactor and stainless steel autoclave were sealed. The autoclave was kept at 2°C for 2 hr and then heated at 100°C in an oven for 2 hr. The obtained slurry was diluted with 200 mL water. With mechanical stirring, H_2O_2 (30%) was dripped into the suspension until the slurry turned golden yellow. The suspension was washed with hot HCl and deionized water until the pH reached 7, and then the hydrated graphene oxide was dissolved in 200 mL deionized water in an Erlenmeyer flask. After ultrasonication for 10 min, the graphene oxide was stored in a refrigerator at 4°C.

1.2.2. Synthesis of Fe_3O_4/graphene oxide

Fe_3O_4/graphene oxide was synthesized by a classical co-precipitation method as follows. $FeCl_3·6H_2O$ (0.017 mol) and $FeSO_4·7H_2O$ (0.0086 mol) were dissolved in 400 mL deionized water mixed with the above prepared graphene oxide (100 mL) under N_2 purging, then the solution was subjected to vigorous mechanical stirring for 60 min. A stoichiometric amount of $NH_3·H_2O$ was added dropwise and stirred for 60 min. The black material was subsequently washed several times to neutral pH. Then the fresh Fe_3O_4/graphene oxide was separated by an external magnet.

1.2.3. Synthesis of Fe^0/Fe_3O_4/graphene

Fe^0/Fe_3O_4/graphene was synthesized by a one-step reduction method under facile conditions. $FeSO_4·7H_2O$ (0.052 mol) was dissolved in 200 mL deionized water and mixed with the fresh Fe_3O_4/graphene oxide under vigorous mechanical stirring for 60 min. A stoichiometric amount of $NaBH_4$ was added dropwise and stirred for 60 min. The black material was subsequently washed several times until neutral pH was achieved. All the above operations were carried out at room temperature. Finally, the fresh Fe^0/Fe_3O_4/graphene was separated by an external magnet and dried in a vacuum oven at 50°C for 24 hr.

1.3. Characterization of Fe^0/Fe_3O_4/graphene

The surface morphology of samples was investigated by using a Hitachi S 4700 scanning electron microscope (SEM) analyzer (Japan) with secondary electron detector at different scales and magnifications. The Fourier transform infrared spectra (FT-IR) were recorded using a FTIR-840OS Shimadzu spectrophotometer (Japan) in the range of 400 to 4000/cm. The X-ray photoelectron spectra (XPS) were measured on an EScalab 250Xi spectrometer (UK) equipped with a XR6 monochromated X-ray source. The magnetic behavior was analyzed by using a Lake Shore 7407 Vibrating Sample Magnetometer (VSM). Specific surface area and porosity of catalyst were measured by nitrogen adsorption/desorption isotherms at 77 K on a BeiShiDe 3H-2000PS2 specific surface and pore size analysis instrument.

1.4. Determination of dye removal

All the batch experiments for dye degradation were conducted in 150 mL beakers. The solution was adjusted with diluted NaOH and H_2SO_4 to the desired initial pH, and the final volume was 100 mL. The desired dosage of Fe^0/Fe_3O_4/graphene was introduced into the reaction solution immediately. Then the beaker was sealed with Parafilm and placed in an electronic stirrer at ambient temperature with continuous stirring. At set intervals, 1.0 mL supernatant of the sample solution was analyzed immediately after separation by an external magnet. Control experiments were also performed under the same conditions.

Determination of dyes was performed by a Shimadzu UV2500 spectrometer (Japan), and the λ_{max} of Methylene Blue, Methyl Orange and Crystal Violet was 664, 464 and 590 nm, respectively.

2. Results and discussion

As shown in Scheme 1, after ultrasonic dispersion in water, the prepared graphene oxide was transformed to exfoliated graphene oxide sheets. A large number of oxygen-containing functional groups existed on the surface of the graphene oxide sheets, which possessed a negatively charged surface in solution and could capture the Fe^{2+} and Fe^{3+} ions through electrostatic interaction. A precipitate formed and the color transformed to black after addition of $NH_3{\cdot}H_2O$. Thus, Fe_3O_4 particles were deposited on the graphene oxide sheets through co-precipitation. The fresh Fe_3O_4/graphene oxide could be dispersed in water due to the hydrophilic nature of Fe_3O_4 and graphene oxide and easily separated from water using a magnet. Moreover, with the remaining functional groups on the surface of the graphene oxide sheets, Fe_3O_4/graphene oxide could capture Fe^{2+} ions in ferrous sulfate solution. After reduction by $NaBH_4$, the trapped Fe^{2+} ions on the graphene oxide surface were transformed to Fe^0 deposited on graphene oxide. Meanwhile, graphene oxide was gradually reduced to graphene with increased addition of $NaBH_4$ and formation of Fe^0. Finally, magnetic Fe^0/Fe_3O_4/graphene with a layered structure was synthesized.

2.1. Characterization of Fe^0/Fe_3O_4/graphene

In order to detect the morphology and structural characteristics of Fe^0/Fe_3O_4/graphene synthesized by the one-step reduction method, SEM, FT-IR, XPS, VSM and nitrogen adsorption/desorption analyses were applied to characterize the Fe^0/Fe_3O_4/graphene composite.

The morphology of Fe^0/Fe_3O_4/graphene is shown in Fig. 1. The planar structure of bare graphene sheets can be observed in Fig. 1a, indicating that the anticipated two-dimensional structure and high surface/volume ratio were obtained (Geng et al., 2011). Significantly, the formation of the layered structure of Fe^0/Fe_3O_4/graphene can be observed in Fig. 1b, with a large number of granular particles tightly attached onto the basal plane of the graphene sheets. Compared with the hydrazine hydrate reduction method, which involved heating to 98°C and produced highly folded graphene sheets (Lv et al., 2014), the preparation of Fe^0/Fe_3O_4/graphene by one-step reduction method was carried out at room temperature, producing clean and flat reduced graphene sheets only

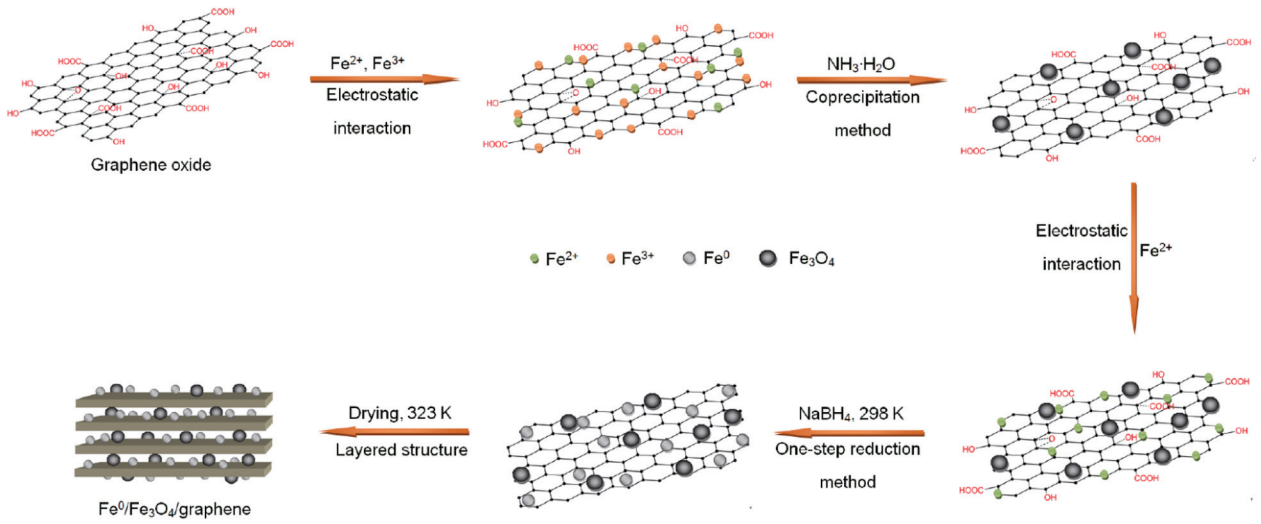

Scheme 1 – Schematic illustration of Fe^0/Fe_3O_4/graphene preparation.

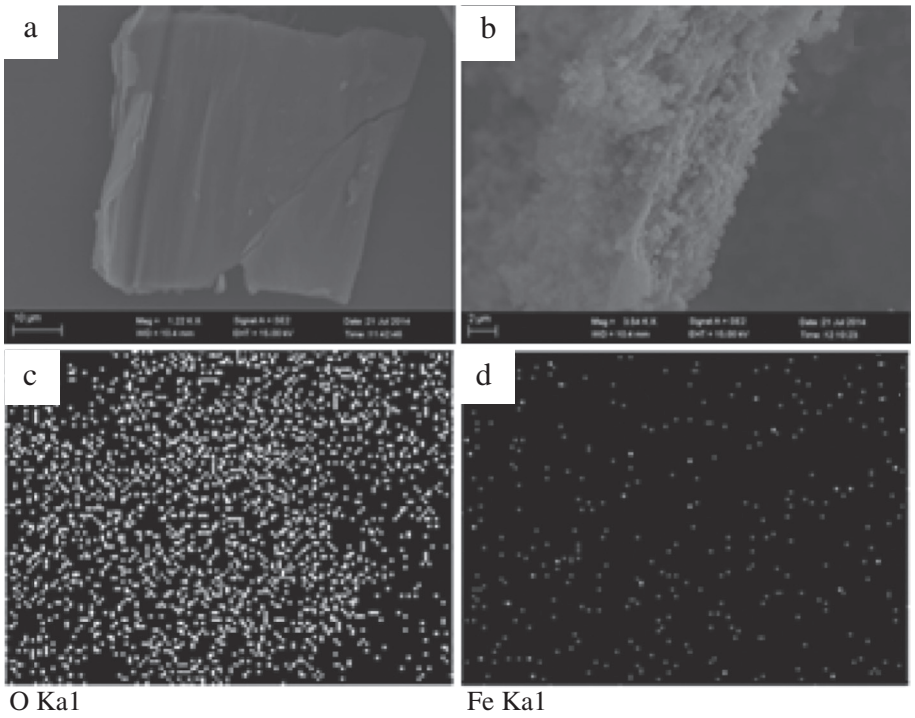

Fig. 1 – Scanning electron microscopy images: (a) graphene; (b) Fe^0/Fe_3O_4/graphene; (c) O element mapping; (d) Fe element mapping.

partially folded at the edge. The O and Fe elements distribution maps in Fe^0/Fe_3O_4/graphene are shown in Fig. 1c and d, respectively. The light spots in Fig. 1c indicate that the O element was on the surface of composite, and the dark spots indicate that the O element was in the inner part of the composite. The O element mainly existed in functional groups on the graphene surface and iron oxides in Fe^0/Fe_3O_4. The dark spots in Fig. 1d are Fe distributed in the composite (Liu et al., 2014). The widespread dark spots indicated that particles of Fe^0 and Fe_3O_4 are highly dispersed in the interlayer of graphene. Thus, Fe crystals had a high level of dispersion in the inner layers of Fe^0/Fe_3O_4/graphene synthesized by the one-step reduction method, so that the agglomeration of Fe^0 and Fe_3O_4 particles was avoided. Therefore, unlike material prepared by other methods, Fe^0/Fe_3O_4/graphene prepared with the one-step reduction method had a layered structure and Fe crystals highly dispersed in the layered gaps, which could enhance the mass transfer process between Fe^0/Fe_3O_4/graphene and the pollutants in water.

The surface bound species of Fe^0/Fe_3O_4/graphene are shown in Fig. 2. The characteristic band of graphene at 1620 cm^{-1} corresponds to the remaining sp^2 character of skeletal vibration (Ahmad et al., 2013). The absorption peaks at 1723, 1384 and 1049 cm^{-1} are ascribed to C═O stretching vibrations, O–H stretching vibrations and C–O stretching vibrations, respectively (Stankovich et al., 2006). The broad peak at 3500–3000 cm^{-1} is attributed to the stretching of the OH groups of adsorbed water (Xing et al., 2011). After reduction by $NaBH_4$ during preparation of Fe^0/Fe_3O_4/graphene, the C═O vibration band disappeared, indicating that reduced graphene was achieved (Guo et al., 2012). In addition, Fe^0/Fe_3O_4/graphene showed the characteristic band of the Fe–O stretching vibration at 594 cm^{-1}, not observed for bare graphene (Ai et al., 2008), indicating that iron oxide was successfully synthesized and deposited on the graphene sheets. The results were similar with those from other preparation methods of Fe^0/Fe_3O_4/graphene (Bhunia et al., 2012; Lv et al., 2014), indicating that Fe_3O_4/graphene and Fe^0 could be synchronously produced by reduction with $NaBH_4$ in the synthesis process.

The chemical composition and chemical states of the elements in Fe^0/Fe_3O_4/graphene were determined by XPS. The XPS survey spectrum of Fe^0/Fe_3O_4/graphene is shown in Fig. 3a. The photoelectron peaks demonstrate the presence of C, O, and Fe elements on the surface. The binding energies at 285 eV, 531 eV, 710 eV and 725 eV were characterized as C 1s, O 1s, Fe $2p_{3/2}$ and Fe $2p_{1/2}$, respectively. In addition to the survey scan, high-resolution scans were obtained for the C 1s, O 1s and Fe 2p regions. Fig. 3b shows the high-resolution XPS C 1s spectra of Fe^0/Fe_3O_4/graphene. Deconvolution of the C 1s peak showed three peaks at 284.8, 285.6 and 288.8 eV, corresponding to C–C, C–O and O–C═O groups, respectively. The peak of O–C═O groups is typical of the spectrum of graphene oxide and generally accounts for the major part of C 1s (Peng et al., 2011). In this C 1s peak, C–C and C–O groups were observed as the main parts of the C 1s peak and O–C═O groups accounted for a small proportion, suggesting that graphene oxide in the composite had been reduced to graphene by $NaBH_4$ effectively (Wang et al., 2014b). The results were similar with those of the FT-IR analysis in Fig. 2. Fig. 3c show the O 1s spectrum, which could be fitted into three peaks at 530.2, 531.1 and 532.1 eV, corresponding to O^{2-}, OH^-, C–O and O–C═O groups, respectively (Xi et al., 2014). The peak of O^{2-} groups was characteristic of lattice oxygen in a metal oxide (Ai et al., 2008), which was in the form of iron

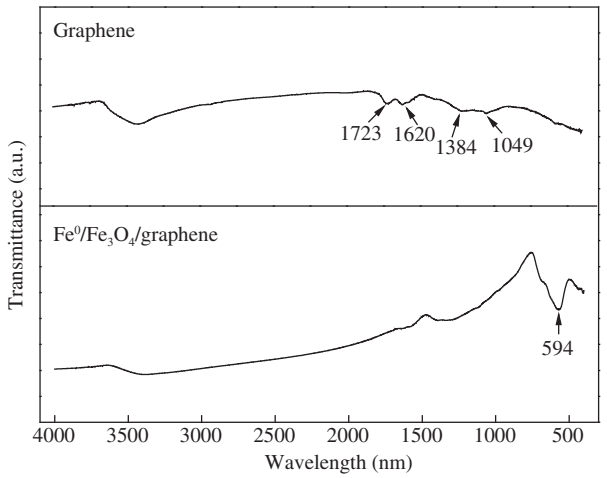

Fig. 2 – Fourier transform infrared spectroscopy spectra of Fe^0/Fe_3O_4/graphene.

oxides in Fe^0/Fe_3O_4/graphene. The peak of OH^- groups was formed by adsorbed oxygen species in the form of iron hydroxides. The peak of C–O and O–C═O groups was consistent with the C 1s spectrum. The high-resolution XPS spectrum of the Fe 2p region is shown in Fig. 3d. The Fe 2p region at binding energies of 710 eV and 725 eV was indexed to Fe $2p_{3/2}$ and Fe $2p_{1/2}$ peaks. The binding energy at 710.5 eV with satellites at 713.3 eV and 727.2 eV could be ascribed to Fe^{2+}, and the binding energy at 724.5 eV with the satellites at 733.6 eV and 717.7 eV could be ascribed to Fe^{3+} in iron oxides (Zhao et al., 2012b). The results were in accordance with the Fe-O analysis of FT-IR and lattice oxygen analysis of O 1s. As seen in Fig. 3d, there was no obvious peak of Fe^0 at 706.7 eV in the Fe 2p region. Since Fe^0 has a tendency to oxidize in air, Fe^0 on the surface of the composite was oxidized in the preparation process (Bhargava et al., 2007). XPS studies the surface of material, thus, the typical Fe^0 peak was not detected. But Fe^0 was still present in the interior of the composite, protected by an external iron oxide film. A similar phenomenon was observed in other related articles (Liu et al., 2014; Lv et al., 2014).

In order to detect the microscopic pore structure of Fe^0/Fe_3O_4/graphene, the sample was measured by a nitrogen adsorption/desorption analysis instrument. The N_2 adsorption–desorption isotherm curve of Fe^0/Fe_3O_4/graphene is shown in Fig. 4. The curve belongs to the Type IV isotherm type according to the International Union of Pure and Applied Chemistry (IUPAC) nomenclature, which indicated the mesoporous structure existing in Fe^0/Fe_3O_4/graphene. The hysteresis loop appeared at p/p^0 = 0.1–1.0, indicating that a capillary condensation phenomenon took place in the mesopore structure. Since the curve did not exhibit any limiting adsorption at high p/p^0, the observed hysteresis could be classified as H3-type. The phenomenon indicated that plate-like particles aggregated and formed

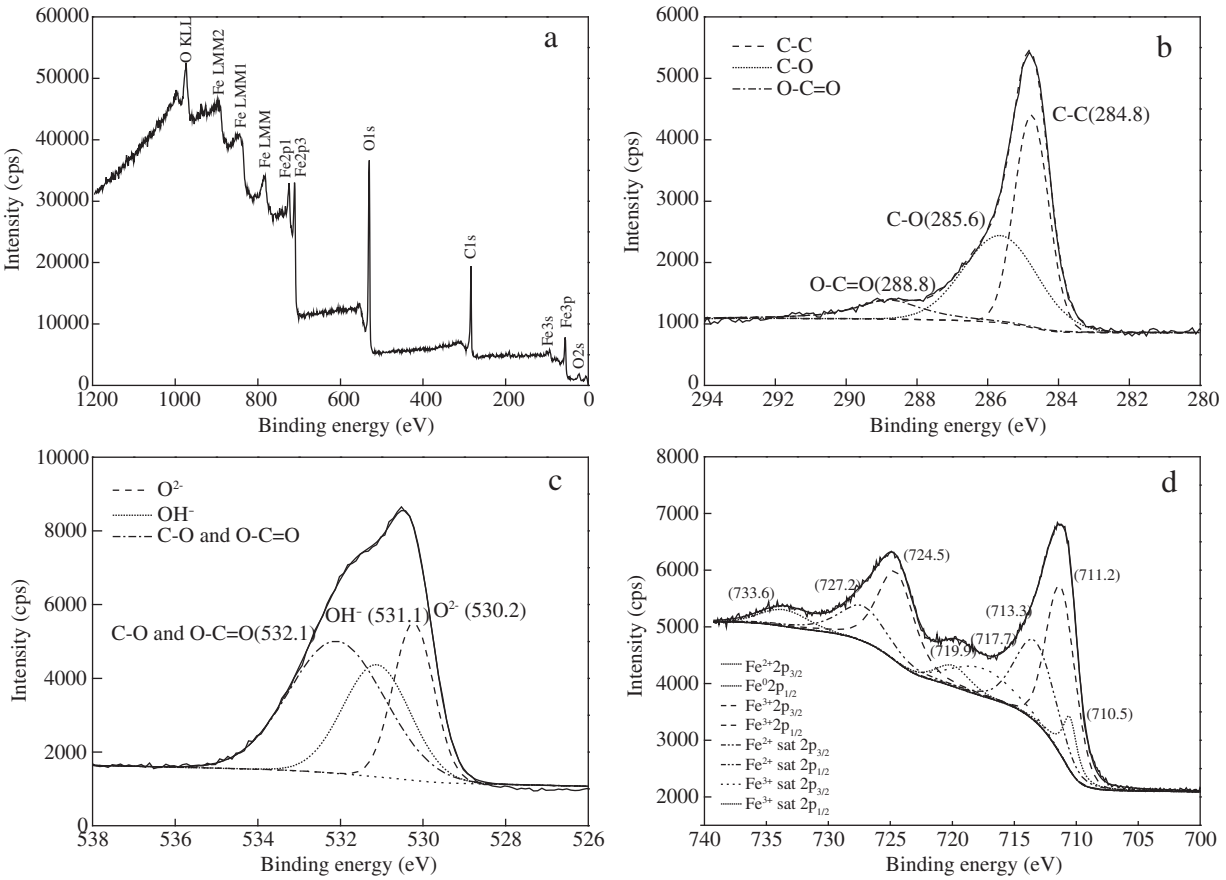

Fig. 3 – X-ray photoelectron spectroscopy spectra of Fe^0/Fe_3O_4/graphene in the (a) survey scan; (b) C1s; (c) O1s; (d) Fe2p energy regions.

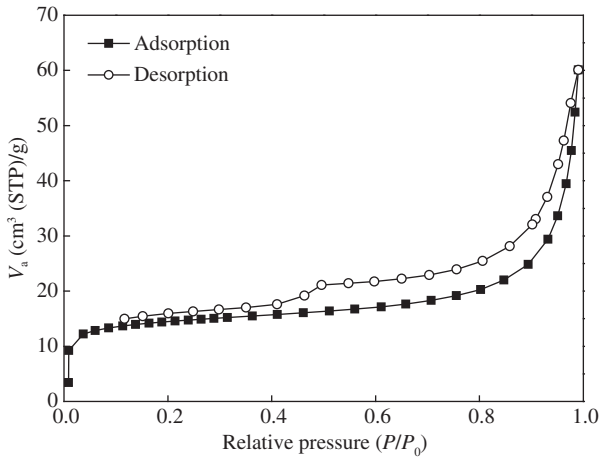

Fig. 4 – N_2 adsorption–desorption isotherms for Fe^0/Fe_3O_4/graphene.

slit-shaped pores in the structure of Fe^0/Fe_3O_4/graphene (Videla et al., 2014). The calculated specific surface area for Fe^0/Fe_3O_4/graphene was approximately equal to 52.91 m^2/g, based on the BET method. The loading of Fe^0 and Fe_3O_4 reduced the specific surface area of graphene compared with other studies (Geng et al., 2011; Yang et al., 2013). The presence of Fe species on the graphene surface could increase the formation of closed-end carbon structures, thus leading to BET value reduction compared to the bare graphene structure (Videla et al., 2014). But beyond that, the lamellar spacing of Fe^0/Fe_3O_4/graphene composite was 22.87 nm, based on the MK-Plate method. Since the average interlayer spacing of graphene is 0.7 nm according to theoretical calculation (Wu et al., 2009), the loading of Fe^0 and Fe_3O_4 particles on the surface of graphene could contribute to the expansion of the slit-shaped pores. The results were in accordance with the layered structure image seen in the SEM analysis in Fig. 1.

In addition to the above characterizations, the magnetic properties of Fe^0/Fe_3O_4/graphene were analyzed to determine whether it has sufficient magnetization to enable fast solid–liquid separation in water treatment. As shown in Fig. 5, a sharp increase in magnetization was observed on increasing the applied field from 0 to 9000 Oe, and the magnetization was saturated at about 2500 Oe. A characteristic ferromagnetic hysteresis loop was also observed from −2500 to 2500 Oe. The saturation magnetization of Fe^0/Fe_3O_4/graphene was 70.394 emu/g, thus it could be easily separated from water by an external magnetic field. The remanence and coercivity of Fe^0/Fe_3O_4/graphene were 3.962 emu/g and 57.316 Oe, respectively. The remanence was low enough that Fe^0/Fe_3O_4/graphene could be easily re-dispersed for reuse after separating from aqueous solution. Therefore, Fe^0/Fe_3O_4/graphene has an advantage over non-magnetic materials for separation, recovery and reuse in water, which has been verified in our study.

2.2. Application of dye removal in water

The dye removal performance of Fe^0/Fe_3O_4/graphene was evaluated in terms of the decolorization efficiencies of dyes. The results are shown in Fig. 6a. Clearly, fast decolorization of Methyl Orange, Methylene Blue and Crystal Violet was achieved after reaction with Fe^0/Fe_3O_4/graphene. The decolorization efficiencies could reach 90.76%, 89.33% and 88.17% in 5 min and stabilize at 94.78%, 91.60% and 89.07% in 20 min, respectively. Compared with existing materials and technologies for the removal of Methyl Orange, Methylene Blue and Crystal Violet in water, Fe^0/Fe_3O_4/graphene removal showed high efficiency in a short time. Most importantly, no additional power input in terms of light, sound, or heat was necessary. For example, Li et al. (2015b) reported that the decolorization efficiency of methyl orange with initial concentration of 10 mg/L was 83% in 10 min by zero-valent copper nanoparticles with dosage of 0.04 g/L in together with hydrodynamic cavitation. Shimizu et al. (2007) reported that the degradation efficiency of methylene blue with initial concentration of 320 mg/L was 95% after 60 min reaction time by 2000 g/L TiO_2 particles together with ultrasound and H_2O_2. Rong et al. (2015) reported that the degradation efficiency of 10 mg/L methylene blue was 98.8% after 100 min reaction time by 0.8 g/L of a TiO_2-graphene photocatalyst, which was prepared from titanium dioxide and graphene oxide by a hydrothermal method. Xia et al. (2014) reported that the degradation efficiencies for 50 mg/L Methyl Orange and Methylene Blue were 95% after 90 min for 1.0 g/L of a Ti-based Layered Double Hydroxide (CeO_2/ZnTi-LDH composite) under visible-light irradiation. Biological treatment, though low cost, generally requires 24 hr or longer to decolorize dyes. Furthermore, the Fe^0/Fe_3O_4/graphene treatment of dyes has the significant advantages of simple operation, easy separation and recycling of the composite, low energy consumption, and safety, without need for the addition of hazardous reagents.

In order to determine which component of Fe^0/Fe_3O_4/graphene played the main role in the decolorization process, the typical UV–Vis spectra of Methyl Orange, Methylene Blue and Crystal Violet during decolorization are shown in Fig. 6b, c, d, respectively. As shown in Fig. 6b, the maximum absorbance band of Methyl Orange was at 464 nm, due to the conjugated structure formed by the azo bond, and the band at 270 nm was ascribed to the π-π transition related to aromatic rings (Galindo et al., 2000). The bands at 465 and 270 nm all became weaker, while a new band at 248 nm appeared after 1 min reaction. This phenomenon indicated that the cleavage of the azo bond occurred and new products formed. The band at 248 nm was possibly ascribable to sulfanilic acid, which has been studied as one of the degradation products of methyl orange (Fan et al., 2009).

For Methylene Blue and Crystal Violet, shown in Fig. 6c and d, there were no obvious new absorbance bands. Similar spectra were also reported in other studies of Methylene Blue and Crystal Violet removal (Arab Chamjangali et al., 2015; Jiang et al., 2015; Lamdab et al., 2015; Wu et al., 2015). It is difficult to identify the major roles in decolorization activities based on UV absorption spectra. In order to investigate which component played a major role in the decolorization process, further study on decolorization performance was carried out by using graphene, Fe_3O_4/graphene and Fe^0/graphene for comparison.

As seen in Fig. 7a, the removal efficiencies of Methyl Orange with graphene and Fe_3O_4/graphene alone were only 18.73% and 18.33% in 40 min, respectively. The removal process was mainly attributed to adsorption by Fe_3O_4 and

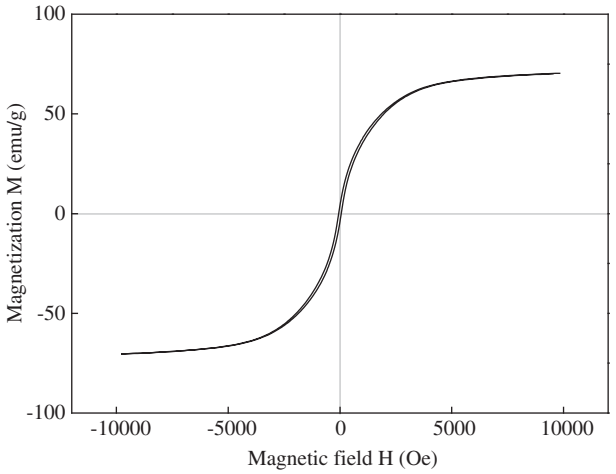

Fig. 5 – Magnetization vs applied magnetic field for Fe^0/Fe_3O_4/graphene.

graphene. By contrast, the removal efficiencies with Fe^0/graphene and Fe^0/Fe_3O_4/graphene alone amounted to 84.18% and 95.60%, respectively. Similar decolorization trends for Methylene Blue and Crystal Violet can be observed in Fig. 7b and c, respectively. These results suggested that reduction by Fe^0 played an important role in the decolorization process. Fe^0/Fe_3O_4/graphene showed the highest activity compared with other samples, indicating that synergetic effects existed in the composite of Fe^0, Fe_3O_4 and graphene.

In addition to the above degradation activities of Fe^0/Fe_3O_4/graphene, the adsorption kinetics of dyes and the composite were also investigated. As shown in Fig. 8, the experiment data were best fitted by the pseudo-second order kinetic model, and the equations can be presented as follows (Zhao et al., 2011):

$$t/q_t = 1/(k_2 q_e^{\,2}) + t/q_e \quad (1)$$

$$q_t = (C_0 - C_t) \times V/M \quad (2)$$

where, q_t (mg/g) and q_e (mg/g) are the adsorption capacity at given time t (min) and at equilibrium, respectively; k_2 (g/(mg·min)) is the adsorption rate constant of the pseudo-second order model; C_0 (mg/L) and C_t (mg/L) are dye concentrations at initial and at given time t (min), respectively; V (L) is the volume of solution; and M (g) is the mass of Fe^0/Fe_3O_4/graphene.

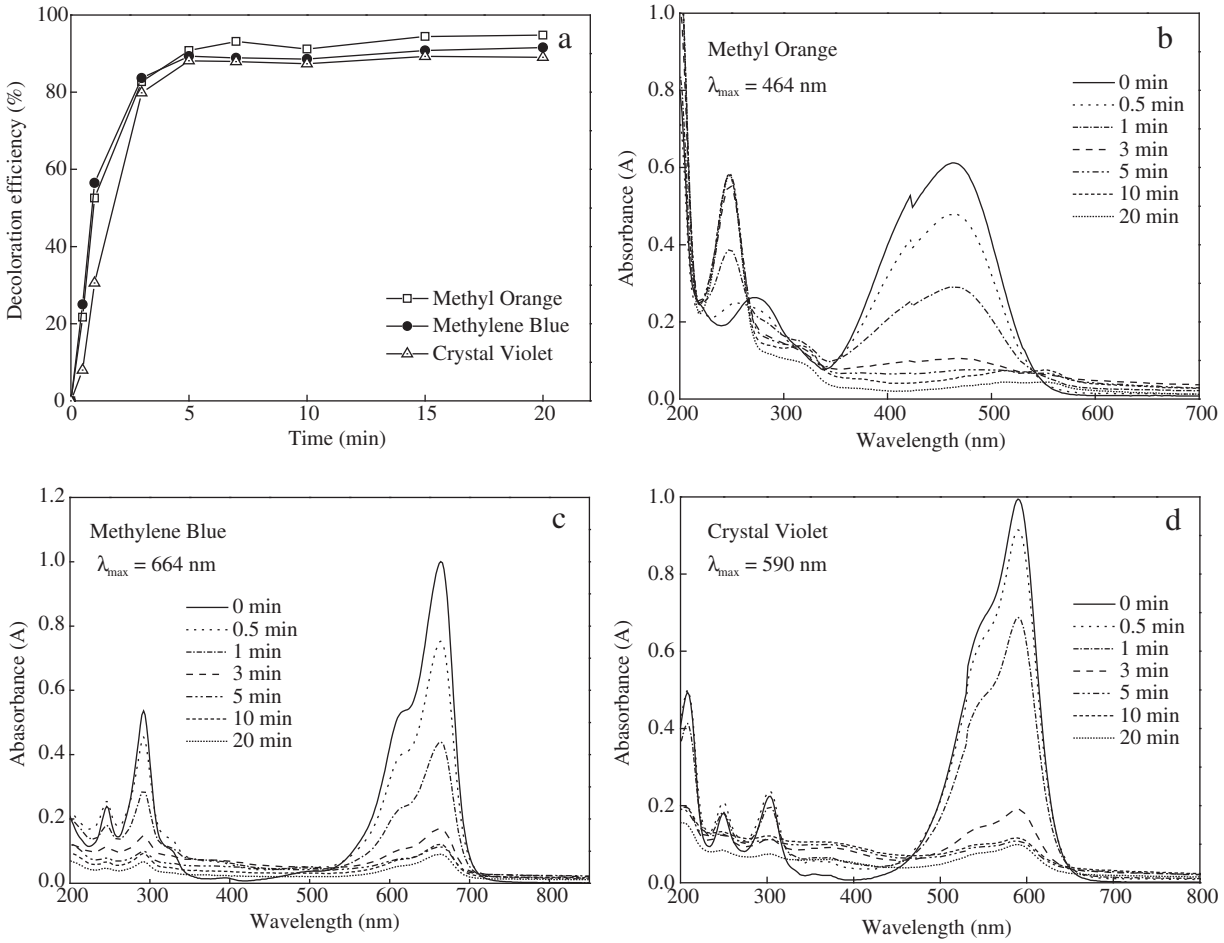

Fig. 6 – UV/Visible adsorption spectra for dye decolorization by Fe^0/Fe_3O_4/graphene: (a) decolorization efficiency *vs.* reaction time; (b) Methyl Orange; (c) Methylene Blue; (d) Crystal Violet. Experimental conditions: concentration of dyes 50 mg/L, pH = 7, Fe^0/Fe_3O_4/graphene dosage = 1.0 g/L, temperature = 298 K.

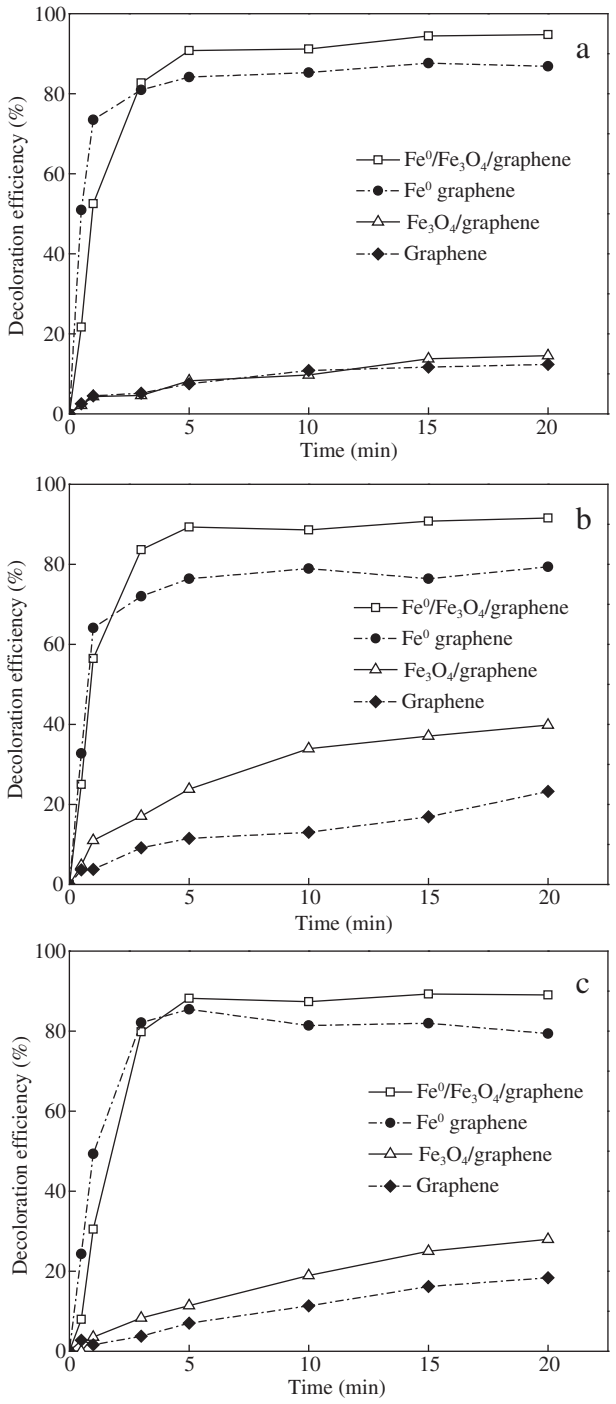

Fig. 7 – Decolorization performance of dyes by different composites: (a) Methyl Orange; (b) Methylene Blue; (c) Crystal Violet. Experimental conditions: concentration of dyes = 50 mg/L, pH = 7, dosage = 1.0 g/L, temperature = 298 K.

The values of correlation coefficients obtained by the pseudo-second-order model for Methyl Orange, Methylene Blue and Crystal Violet were all higher than 0.95, suggesting that adsorption by Fe^0/Fe_3O_4/graphene indeed took place and played an important role in the reaction process. The adsorption rate constants of Methyl Orange, Methylene Blue and Crystal Violet were 2.440, 2.220 and 1.816 g/(mg·min), respectively. The fast adsorption rates might be attributed to

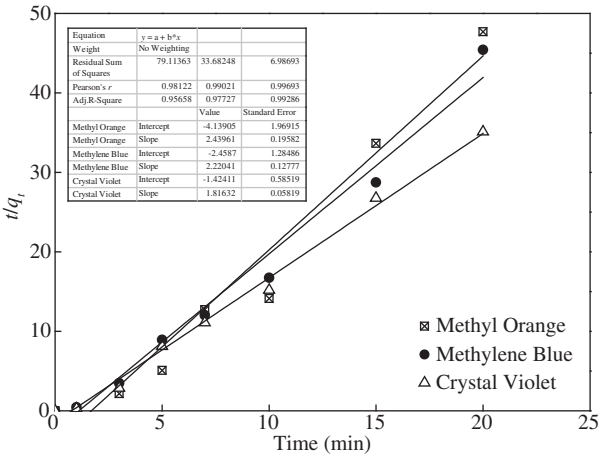

Fig. 8 – Pseudo-second-order kinetic plots for the adsorption of dyes.

the strong adsorption ability of graphene and Fe_3O_4 particles deposited on the graphene sheets. Thus, dye molecules could be adsorbed on the composite of Fe^0/Fe_3O_4/graphene first, then dye molecules were degraded and intermediates were generated. Finally, part of the intermediates was released to solution, regenerating the active sites to absorb more dye molecules. Therefore, the dye removal efficiencies increased rapidly in the initial stage due to simultaneous adsorption and degradation by Fe^0/Fe_3O_4/graphene in water.

Based on the analysis of the reaction process and relevant literature, the mechanism for dye removal by Fe^0/Fe_3O_4/graphene in water was deduced. At the beginning of reaction, the transformation of Fe^0 on graphene may occur as follows (Eqs. (3) and (4)) (Hung et al., 2000; Cheng et al., 2007; Liang et al., 2014).

$$Fe^0 + 2H_2O \rightarrow Fe^{2+} + H_2 + 2OH^- \quad (3)$$

$$2Fe^0 + 2H_2O + O_2 \rightarrow 2Fe^{2+} + 4OH^-. \quad (4)$$

The generated Fe^{2+} would undergo further oxidation in the presence of oxygen (Eq. (5)) (Crane and Scott, 2012; Zhang et al., 2012). Then, the oxidized Fe^{3+} species were reduced to Fe^{2+} species by Fe^0 in the composite. In addition, the electrons would be transferred from Fe^0 to Fe^{3+} on the magnetite to generate Fe^{2+}, and then more Fe^{2+} at octahedral sites was formed (Eq. (6)) (Costa et al., 2008; Dos Santos Coelho et al., 2008).

$$4Fe^{2+} + 2H_2O + O_2 \rightarrow 4Fe^{3+} + 4OH^- \quad (5)$$

$$Fe^0 + 2Fe^{3+} \rightarrow 3Fe^{2+}. \quad (6)$$

In neutral or alkaline solutions, the formation of iron hydroxides occurred as follows (Eqs. (7) and (8)) (Cheng et al., 2007; Triszcz et al., 2009). Thus, $Fe(OH)_2$ or $Fe(OH)_3$ could be formed on the surface of Fe^0/Fe_3O_4/graphene.

$$Fe^{2+} + 2OH^- \rightarrow Fe(OH)_2 \quad (7)$$

$$Fe^{3+} + 3H_2O \rightarrow Fe(OH)_3 + H^+. \quad (8)$$

The graphene in the composite had adsorption ability through π–π interaction with dye molecules, and the iron hydroxides and Fe_3O_4 formed in the composite could also adsorb dye molecules through electrostatic interaction; thus, the dye molecules tended to aggregate in the composite. Then, the adsorbed dye molecules became much easier to reduce by Fe^0. Since multiple electron transfer pathways existed in the composite due to the synergistic effects of Fe^0, Fe_3O_4 and graphene, the reduction process could be enhanced. In our study, adsorption and enhanced reduction by Fe^0/Fe_3O_4/graphene may play important roles in the removal of dyes in water.

3. Conclusions

This study demonstrated that Fe^0/Fe_3O_4/graphene was successfully synthesized by a one-step reduction method under facile conditions. Distinct from material prepared by other methods, Fe^0/Fe_3O_4/graphene prepared by the one-step reduction method possessed a layered structure and Fe crystals highly dispersed in the interlayer of the planar graphene sheets. In addition, the composite with its ferromagnetism could be easily separated and re-dispersed for reuse in water. Furthermore, Fe^0/Fe_3O_4/graphene exhibited a fast decolorization rate and high removal efficiency for typical dyes in water. After 20 min of reaction, the removal efficiencies of Methyl Orange, Methylene Blue and Crystal Violet were 94.78%, 91.60% and 89.07%, respectively. In summary, Fe^0/Fe_3O_4/graphene has potential application in removal of dyes in water, which would contribute to the development of water treatment technologies for refractory dyes.

Acknowledgments

This work was supported by the Fundamental Research Funds for Central Universities and Research Funds of Renmin University of China (Nos. 14XLNQ02, 15XNLD04).

REFERENCES

Ahmad, M., Ahmed, E., Hong, Z.L., Xu, J.F., Khalid, N.R., Elhissi, A., Ahmed, W., 2013. A facile one-step approach to synthesizing ZnO/graphene composites for enhanced degradation of methylene blue under visible light. Appl. Surf. Sci. 274, 273–281.

Ai, Z., Cheng, Y., Zhang, L., Qiu, J., 2008. Efficient removal of Cr(VI) from aqueous solution with $Fe@Fe_2O_3$ core-shell nanowires. Environ. Sci. Technol. 42 (18), 6955–6960.

Arab Chamjangali, M., Bagherian, G., Javid, A., Boroumand, S., Farzaneh, N., 2015. Synthesis of Ag–ZnO with multiple rods (multipods) morphology and its application in the simultaneous photo-catalytic degradation of methyl orange and methylene blue. Spectrochim. Acta A 150, 230–237.

Bao, C.L., Song, L., Xing, W.Y., Yuan, B.H., Wilkie, C.A., Huang, J.L., Guo, Y.Q., Hu, Y., 2012. Preparation of graphene by pressurized oxidation and multiplex reduction and its polymer nanocomposites by masterbatch-based melt blending. J. Mater. Chem. 22 (13), 6088–6096.

Bhargava, G., Gouzman, I., Chun, C.M., Ramanarayanan, T.A., Bernasek, S.L., 2007. Characterization of the "native" surface thin film on pure polycrystalline iron: A high resolution XPS and TEM study. Appl. Surf. Sci. 253 (9), 4322–4329.

Bhunia, P., Kim, G., Baik, C., Lee, H., 2012. A strategically designed porous iron–iron oxide matrix on graphene for heavy metal adsorption. Chem. Commun. 48 (79), 9888–9890.

Chen, H.W., Kuo, Y.L., Chiou, C.S., You, S.W., Ma, C.M., Chang, C.T., 2010. Mineralization of reactive black 5 in aqueous solution by Ozone/H_2O_2 in the presence of a magnetic catalyst. J. Hazard. Mater. 174 (1–3), 795–800.

Cheng, R., Wang, J.L., Zhang, W.X., 2007. Comparison of reductive dechlorination of p-chlorophenol using Fe^0 and nanosized Fe^0. J. Hazard. Mater. 144 (1–2), 334–339.

Costa, R.C.C., Moura, F.C.C., Ardisson, J.D., Fabris, J.D., Lago, R.M., 2008. Highly active heterogeneous fenton-like systems based on Fe^0/Fe_3O_4 composites prepared by controlled reduction of iron oxides. Appl. Catal. B Environ. 83 (1–2), 131–139.

Crane, R.A., Scott, T.B., 2012. Nanoscale zero-valent iron: Future prospects for an emerging water treatment technology. J. Hazard. Mater. 211, 112–125.

Dos Santos Coelho, F., Ardisson, J.D., Moura, F.C.C., Lago, R.M., Murad, E., Fabris, J.D., 2008. Potential application of highly reactive Fe^0/Fe_3O_4 composites for the reduction of Cr(VI) environmental contaminants. Chemosphere 71 (1), 90–96.

Fan, J., Guo, Y., Wang, J., Fan, M., 2009. Rapid decolorization of azo dye methyl orange in aqueous solution by nanoscale zerovalent iron particles. J. Hazard. Mater. 166 (2–3), 904–910.

Galindo, C., Jacques, P., Kalt, A., 2000. Photodegradation of the aminoazobenzene acid orange 52 by three advanced oxidation processes: UV/H_2O_2 UV/TiO_2 and Vis/TiO_2-comparative mechanistic and kinetic investigations. J. Photochem. Photobiol. A Chem. 130 (1), 35–47.

Geng, D., Yang, S., Zhang, Y., Yang, J., Liu, J., Li, R., Sham, T.K., Sun, X., Ye, S., Knights, S., 2011. Nitrogen doping effects on the structure of graphene. Appl. Surf. Sci. 257 (21), 9193–9198.

Guo, J., Wang, R., Tjiu, W.W., Pan, J., Liu, T., 2012. Synthesis of fe nanoparticles@graphene composites for environmental applications. J. Hazard. Mater. 225, 63–73.

Guo, S., Zhang, G., Guo, Y., Yu, J.C., 2013. Graphene oxide-Fe_2O_3 hybrid material as highly efficient heterogeneous catalyst for degradation of organic contaminants. Carbon 60, 437–444.

Hung, H.M., Ling, F.H., Hoffmann, M.R., 2000. Kinetics and mechanism of the enhanced reductive degradation of nitrobenzene by elemental iron in the presence of ultrasound. Environ. Sci. Technol. 34 (9), 1758–1763.

Ishigami, M., 2007. Atomic structure of graphene on SiO_2. Nano Lett. 7 (6), 1643–1648.

Jabeen, H., Kemp, K.C., Chandra, V., 2013. Synthesis of nano zerovalent iron nanoparticles — graphene composite for the treatment of lead contaminated water. J. Environ. Manag. 130, 429–435.

Jiang, Y.R., Lin, H.P., Chung, W.H., Dai, Y.M., Lin, W.Y., Chen, C.C., 2015. Controlled hydrothermal synthesis of BiOxCly/BiOmIn, composites exhibiting visible-light photocatalytic degradation of crystal violet. J. Hazard. Mater. 283, 787–805.

Kusic, H., Leszczynska, D., Koprivanac, N., Peternel, I., 2011. Role of quantum dots nanoparticles in the chemical treatment of colored wastewater: catalysts or additional pollutants. J. Environ. Sci. 23 (9), 1479–1485.

Lamdab, U., Wetchakun, K., Phanichphant, S., Kangwansupamonkon, W., Wetchakun, N., 2015. Highly efficient visible light-induced photocatalytic degradation of methylene blue over $InVO_4/BiVO_4$ composite photocatalyst. J. Mater. Sci. 50 (17), 5788–5798.

Li, J., Zhang, S., Chen, C., Zhao, G., Yang, X., Li, J., Wang, X., 2012. Removal of Cu(II) and fulvic acid by graphene oxide nanosheets

decorated with Fe_3O_4 nanoparticles. ACS Appl. Mater. Interfaces 4 (9), 4991–5000.
Li, J., Shao, Z., Chen, C., Wang, X., 2014. Hierarchical GOs/Fe_3O_4/PANI magnetic composites as adsorbent for ionic dye pollution treatment. RSC Adv. 4 (72), 38192–38198.
Li, J., Chen, C., Zhang, R., Wang, X., 2015a. Nanoscale zero-valent iron particles supported on reduced graphene oxides by using a plasma technique and their application for removal of heavy-metal ions. Chem. Asian. J. 10 (6), 1410–1417.
Li, P., Song, Y., Wang, S., Tao, Z., Yu, S., Liu, Y., 2015b. Enhanced decolorization of methyl orange using zero-valent copper nanoparticles under assistance of hydrodynamic cavitation. Ultrason. Sonochem. 22, 132–138.
Liang, L., Sun, W., Guan, X., Huang, Y., Choi, W., Bao, H., Li, L., Jiang, Z., 2014. Weak magnetic field significantly enhances selenite removal kinetics by zero valent iron. Water Res. 49, 371–380.
Liu, M., Wen, T., Wu, X., Chen, C., Hu, J., Li, J., Wang, X., 2013. Synthesis of porous Fe_3O_4 hollow microspheres/graphene oxide composite for Cr(VI) removal. Dalton Trans. 42 (41), 14710–14717.
Liu, F., Yang, J., Zuo, J., Ma, D., Gan, L., Xie, B., Wang, P., Yang, B., 2014. Graphene-supported nanoscale zero-valent iron: removal of phosphorus from aqueous solution and mechanistic study. J. Environ. Sci. 26 (8), 1751–1762.
Lv, X., Xue, X., Jiang, G., Wu, D., Sheng, T., Zhou, H., Xu, X., 2014. Nanoscale zero-valent iron (nZVI) assembled on magnetic Fe_3O_4/graphene for chromium (VI) removal from aqueous solution. J. Colloid Interface Sci. 417, 51–59.
Netpradit, S., Thiravetyan, P., Towprayoon, S., 2004. Adsorption of three azo reactive dyes by metal hydroxide sludge: effect of temperature, pH, and electrolytes. J. Colloid Interface Sci. 270 (2), 255–261.
Nguyen, T.D., Phan, N.H., Do, M.H., Ngo, K.T., 2011. Magnetic Fe(2)MO(4) (M: Fe, Mn) activated carbons: fabrication, characterization and heterogeneous fenton oxidation of methyl orange. J. Hazard. Mater. 185 (2–3), 653–661.
Noroozi, B., Sorial, G.A., 2013. Applicable models for multi-component adsorption of dyes: a review. J. Environ. Sci. (China) 25 (3), 419–429.
Padamavathy, S., Sandhya, S., Swaminathan, K., Subrahmanyam, Y.V., Kaul, S.N., 2003. Comparison of decolorization of reactive azo dyes by microorganisms isolated from various sources. J. Environ. Sci. (China) 15 (5), 628–632.
Peng, X.Y., Liu, X.X., Diamond, D., Lau, K.T., 2011. Synthesis of electrochemically-reduced graphene oxide film with controllable size and thickness and its use in supercapacitor. Carbon 49 (11), 3488–3496.
Rong, X., Qiu, F., Zhang, C., Fu, L., Wang, Y., Yang, D., 2015. Preparation, characterization and photocatalytic application of TiO_2-graphene photocatalyst under visible light irradiation. Ceram. Int. 41 (2), 2502–2511.
Shimizu, N., Ogino, C., Dadjour, M.F., Murata, T., 2007. Sonocatalytic degradation of methylene blue with TiO_2 pellets in water. Ultrason. Sonochem. 14 (2), 184–190.
Stankovich, S., Piner, R.D., Nguyen, S.T., Ruoff, R.S., 2006. Synthesis and exfoliation of isocyanate-treated graphene oxide nanoplatelets. Carbon 44 (15), 3342–3347.
Sun, Y., Ding, C., Cheng, W., Wang, X., 2014. Simultaneous adsorption and reduction of U(VI) on reduced graphene oxide-supported nanoscale zerovalent iron. J. Hazard. Mater. 280, 399–408.
Triszcz, J.M., Port, A., Einschlag, F.S.G., 2009. Effect of operating conditions on iron corrosion rates in zero-valent iron systems for arsenic removal. Chem. Eng. J. 150 (2–3), 431–439.
Videla, A.H.A.M., Ban, S., Specchia, S., Zhang, L., Zhang, J., 2014. Non-noble Fe–N-x electrocatalysts supported on the reduced graphene oxide for oxygen reduction reaction. Carbon 76, 386–400.
Wang, Y., Polavarapu, L., Liz-Marzan, L.M., 2014a. Reduced graphene oxide-supported gold nanostars for improved sers sensing and drug delivery. ACS Appl. Mater. Interfaces 6 (24), 21798–21805.
Wang, C., Luo, H., Zhang, Z., Wu, Y., Zhang, J., Chen, S., 2014b. Removal of As(III) and As(V) from aqueous solutions using nanoscale zero valent iron-reduced graphite oxide modified composites. J. Hazard. Mater. 268, 124–131.
Wu, J., Gao, H., Yao, S., Chen, L., Gao, Y., Zhang, H., 2015. Degradation of crystal violet by catalytic ozonation using fe/activated carbon catalyst. Sep. Purif. Technol. 147, 179–185.
Wu, Z.S., Ren, W.C., Gao, L.B., Liu, B.L., Jiang, C.B., Cheng, H.M., 2009. Synthesis of high-quality graphene with a pre-determined number of layers. Carbon 47 (2), 493–499.
Xi, Y., Sun, Z., Hreid, T., Ayoko, G.A., Frost, R.L., 2014. Bisphenol a degradation enhanced by air bubbles via advanced oxidation using in situ generated ferrous ions from nano zero-valent iron/palygorskite composite materials. Chem. Eng. J. 247, 66–74.
Xia, S.J., Liu, F.X., Ni, Z.M., Shi, W., Xue, J.L., Qian, P.P., 2014. Ti-based layered double hydroxides: efficient photocatalysts for azo dyes degradation under visible light. Appl. Catal. B Environ. 144, 570–579.
Xing, S., Zhou, Z., Ma, Z., Wu, Y., 2011. Characterization and reactivity of Fe_3O_4/FeMnOx core/shell nanoparticles for methylene blue discoloration with H_2O_2. Appl. Catal. B Environ. 107 (3–4), 386–392.
Yang, X., Qin, J., Li, Y., Zhang, R., Tang, H., 2013. Graphene-spindle shaped TiO_2 mesocrystal composites: Facile synthesis and enhanced visible light photocatalytic performance. J. Hazard. Mater. 261, 342–350.
Zhang, P.Y., Zhang, G.M., Dong, J.H., Fan, M.H., Zeng, G.M., 2012. Bisphenol a oxidative removal by ferrate (Fe(VI)) under a weak acidic condition. Sep. Purif. Technol. 84, 46–51.
Zhang, W., Shi, X., Zhang, Y., Gu, W., Li, B., Xian, Y., 2013. Synthesis of water-soluble magnetic graphene nanocomposites for recyclable removal of heavy metal ions. J. Mater. Chem. A 1 (5), 1745–1753.
Zhao, D., Sheng, G., Hu, J., Chen, C., Wang, X., 2011. The adsorption of Pb(II) on Mg_2Al layered double hydroxide. Chem. Eng. J. 171 (1), 167–174.
Zhao, D., Sheng, G., Chen, C., Wang, X., 2012a. Enhanced photocatalytic degradation of methylene blue under visible irradiation on graphene@TiO_2 dyade structure. Appl. Catal. B Environ. 111, 303–308.
Zhao, H., Wang, Y., Wang, Y., Cao, T., Zhao, G., 2012b. Electro-fenton oxidation of pesticides with a novel Fe_3O_4@ Fe_2O_3/activated carbon aerogel cathode: high activity, wide pH range and catalytic mechanism. Appl. Catal. B Environ. 125, 120–127.
Zhao, H., Zhang, G., Zhang, Q., 2014. MnO_2/CeO_2 for catalytic ultrasonic degradation of methyl orange. Ultrason. Sonochem. 21 (3), 991–996.
Zubir, N.A., Yacou, C., Motuzas, J., Zhang, X., Diniz da Costa, J.C., 2014. Structural and functional investigation of graphene oxide-Fe_3O_4 nanocomposites for the heterogeneous Fenton-like reaction. Sci. Rep. 4, 4594.